L-Cysteine-Assisted Synthesis of PbS Nanocube-Based Pagoda-like Hierarchical Architectures

Fan Zuo, Si Yan, Bin Zhang, Yu Zhao, and Yi Xie*

Department of Nanomaterials and Nanochemistry, Hefei National Laboratory for Physical Sciences at Microscale, University of Science and Technology of China, Hefei, Anhui 230026, P. R. China

Received: August 17, 2007; In Final Form: December 11, 2007

Nanocube-based pagoda-like PbS hierarchical architectures have been fabricated by hydrothermal treatment of $Pb(Ac)_2$ and L-cysteine solution. It was suggested that a biomimetic mineralization process happened during the growth of the hierarchical architectures. The biomolecule, L-cysteine, exerts coordination, oriented nucleation of crystals, and the morphology modulating effect. By studying the intermediates of the reaction, we observed that 4-fold symmetric star-shaped microcrystals were formed at first, and a second nucleation process resulted in the generation of nanocube-based pagoda-like hierarchical architectures. By varying the concentration of the reaction system, we got PbS nanocubes and octahedron microcystals. The morphology evolutions of PbS materials are explained by the growth rule of fcc nanocrystals. This facile L-cysteine-assisted technique is expected to be employed for the shape-controlled synthesis of other fcc structural nanomaterials.

1. Introduction

The intrinsic properties of nanomaterials are determined not only by their chemical composition but also by their shape and size.[1−3] During recent years, the development of nanotechnology enabled us to synthesize nanoscaled materials including metals, semiconductors, hybrid materials, and so forth, whose size can be controlled from 1 nm to 1 μm in many cases.[4−7] Size-tunable nanounits can be served as ideal building blocks for the hierarchical architectures of functional nanoscaled devices that could eventually overcome the fundamental and economic limitations of conventional lithography-based fabrication.[7−11] Constructing complex architectures from small building blocks is common in nature. Shells, diatoms, bones, and teeth are delicate examples of well-defined structures, formed as a result of biomineralization by using organic templates to control the growth of the inorganic phase.[12−18] These natural hierarchical materials usually possess remarkably optimized properties such as mechanical stiffness, light conduction, or even multifunctions at wide length scales.[16,19] In the realm of biomineralization, the principal concept is that organized biomacromolecules, containing well-defined arrays of functional groups, command polymorph selection and the oriented nucleation of crystals by lowering the nucleation energy of specific crystal faces. The crystal morphology is then controlled by the interaction of biomolecules in solution with specific crystal planes during growth.[20,21] Inspired by this concept, many biologists and materials scientists dedicated to mimic the biomineralization process to design and fabricate artificial crystals with potential applications in nanomaterials science and biotechnology. For example, surfactants and macromolecules have been used to prepare hierarchical architectures, whose properties are determined by both the building blocks and the morphology of the architectures.[3,11,22] It is generally accepted that hierarchical structures are formed through the oriented attachment of building blocks. Recently, a novel second nucleation process is reported and used to explain the growth of the hierarchical architectures.[23] Huang et al. have observed the second nucleation of PbS nuclei in the formation of hierarchical PbS hollow microcrystals.[3] Because the architectural control of nanoparticles with well-defined shapes is the crux to guide these nanoscaled building blocks to ordered superstructures, assemblies, or complex buildings, which have been found to be prospective units of future nanoscaled electronic and optoelectronic devices, the ability to understand and predict the final architecture of these nanoscaled building blocks shows significant importance. If the growth mechanism and the shape-guiding process could be understood, then we would be able to anticipate constructing the building blocks with desired shape and crystallinity.

Lead sulfide (PbS) is a well-known $\pi-\pi$ semiconductor material with a small band gap (0.41 eV in bulk form, at 300K) and a very large exciton Bohr radius (18 nm), which contribute to the strong quantum-confinement effect over a large nanocrystalline size range. Therefore, nanoscaled PbS has shown some novel and excellent optical and electronic properties, such as IR photodetectors, photovoltaics, electroluminescence, photoluminescence, thermal and biological images, and display devices.[24−26] Also, PbS quantum-dot doped glasses can be used as saturable absorbers for the mode locking of a Cr:forsterite laser, a solar absorber, and for photography.[28] Moreover, it has been expected that the third-order nonlinear optical response of PbS nanocrystals is 30 times larger than that of GaAs and 1000 times larger than that of CdSe, which makes PbS nanocrystals a promising candidate for photonic and optical switching device applications.[27] Although PbS nano- and microcrystals with various morphologies such as dendrites, multipods, polydedrons, and nanobelts[24−31] have been achieved, the development of conceptually simple, environmentally friendly, and universal construction techniques for large-scale fabrication of hierarchical PbS crystals with complex patterns but ordered assemblies is expected to be further developed.

* Corresponding author. E-mail: yxie@ustc.edu.cn. Fax: (+86)551-360-3987.

10.1021/jp0766149 CCC: $40.75
Published on Web 02/01/2008

Biomolecule-assisted synthesis has been proven to be a novel, environmentally friendly, and promising method in the preparation of various nanomaterials owing to its convenience and strong function in morphology control. For example, branched CdTe wires have been successfully synthesized by using amphiphilic biomolecules as templates.[32] Komarneni et al. have used Glutathione (GSH) as both assembling molecules and the sulfur source to synthesize snowflake-like bismuth sulfide nanorods under microwave irradiation.[33] Starch has also been introduced to serve as the reducing and morphology-directing agent for the preparation of tellurium nanowires.[34] Recently, we have reported the porous spongy-like Ni_3S_2 and network-like MnS nanostructures by the assistance of L-cysteine ($HSCH_2$-$CH(NH_2)COOH$).[35,36] Herein, we report a nanocube-based pagodalike hierarchical architecture of PbS achieved through an L-cysteine-assisted strategy. This strategy is inspired by the fact that L-cysteine contains plenty of functional groups, which may exert similar polymorph selection, oriented nucleation of crystals, and morphology modulating effect occurring in biomineralization. To the best of our knowledge, it is the first time that such a hierarchical architecture among various micro-/nanostructures has been reported. The formation mechanism study suggests that a second nucleation process during the growth process is responsible for the formation of such a hierarchical architecture. Further study shows that different morphologies of the final products can be controlled effectively simply by adjusting the concentration of the reactants.

2. Experimental Section

All of the chemicals are of analytical grade and used as received. In a typical experiment, $Pb(Ac)_2$ (0.152 g) and L-cysteine (0.097 g) with a 1:2 molar ratio were dissolved in 15 mL and 25 mL of deionized water. Then $Pb(Ac)_2$ solution was added to the L-cysteine solution under constant stirring. The mixed solution became a grayish-green suspension immediately. After stirring for 20 min, the suspension was transferred into a Teflon-lined stainless-steel autoclave with a capacity of 60 mL. The autoclave was sealed and maintained at 120 °C for 6 h and then cooled to room temperature naturally. The precipitate was collected and washed with distilled water and absolute ethanol for three times, respectively. Then, the samples were dried in a vacuum at 50 °C for 6 h and the pink powders were obtained.

The X-ray diffraction patterns (XRD) of the products were recorded with a Rigaku Dmax Diffraction System using a Cu Kα source ($\lambda = 0.154178$ nm). The field emission scanning electron microscopy (FESEM) images were taken with a JEOL-JSM-6700F field emission scanning electron microscope (FE-SEM, 15 kV). Transmission electron microscopy (TEM) images were obtained with Hitachi 800 system at 200 kV. The HR-TEM images and the corresponding SAED patterns were taken on a JEOL 2010 high-resolution TEM performing at 200 kV. Energy-dispersive X-ray spectroscopy (EDX) analysis was performed on a JEOL-2010 high-resolution electron microscope equipped with the EX24095JGT energy-dispersion X-ray fluorescence analyzer. The Fourier transform infrared (FTIR) spectroscopic study was carried out with a MAGNA-IR 750 (Nicolet Instrument Co.) FTIR spectrometer.

3. Results and Discussion

The phase and purity of the as-obtained product is characterized by XRD analysis as shown in Figure 1. All of the diffraction peaks can be indexed as cubic PbS with a lattice constant of $a = 5.931$ Å (JCPDS 78-1901). The morphology of the as-prepared PbS is examined by field emission scanning electron microscopy (FESEM). Figure 2a shows a panoramic FESEM image of the product obtained at 120 °C for 6 h, which presents a novel pagoda-like architecture with a diagonal length of ca. 2 μm. The product consists almost entirely of such pagoda-like architectures, giving the information that high yield and good uniformity can be readily achieved through this approach. Figure 2b viewed from the frontal perspective shows an individual pagoda-like architecture that has six arms with high geometrical symmetry. The FESEM images (Figure 2c and d) with higher magnification clearly show that the pagoda-like architectures are composed of numerous nanocubes aligned face-to-face. Figure 2c clearly shows a three-dimensional "layered" structure. Each arm contains a main "trunk" constructed from big nanocubes with smaller nanocubes growing out on the tops of the big cubes and between the adjacent "layers". The length of the nanocubes ranges from 20 to 50 nm as shown in Figure 2d, and the closer to the tip of the arm, the smaller the nanocubes become.

The crystallinity is examined by high-resolution transmission electron microscopy (HRTEM) and selected-area electron dif-

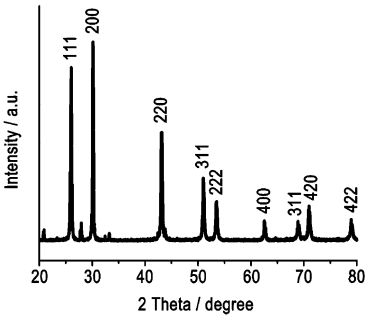

Figure 1. XRD pattern of the prepared nanocube-based pagoda-like hierarchical architectures of the PbS, synthesized from 0.152 g of $Pb(Ac)_2$ and 0.097 g of L-cysteine (with a 1:2 molar ratio) dissolved in 40 mL of deionized water maintaining at 120 °C for 6 h. The diffraction peaks indicate that the product is phase-pure cubic PbS with high crystallinity.

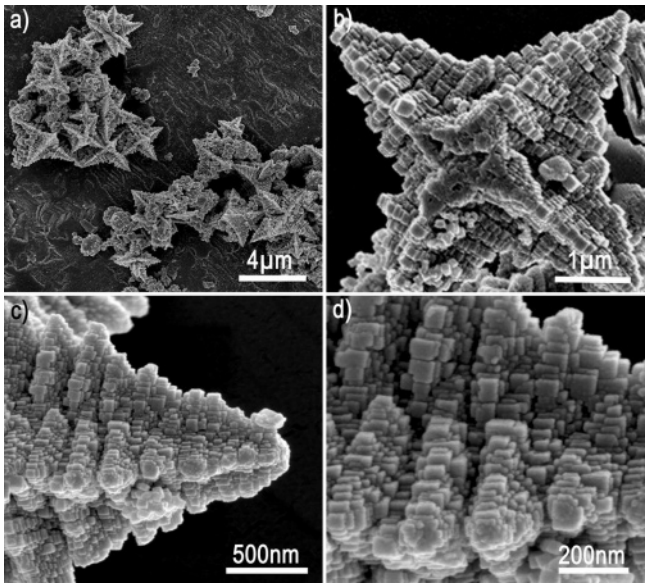

Figure 2. FESEM images of the as-synthesized PbS hierarchical architectures at different magnifications. (a) Low-magnification FESEM image, showing the high yield and uniform size distribution. (b) An individual architecture viewed from the frontal perspective. (c and d) High-magnification FESEM image of the architecture showing the arm with a layered structure and the nanocube-based building blocks of the architecture, respectively.

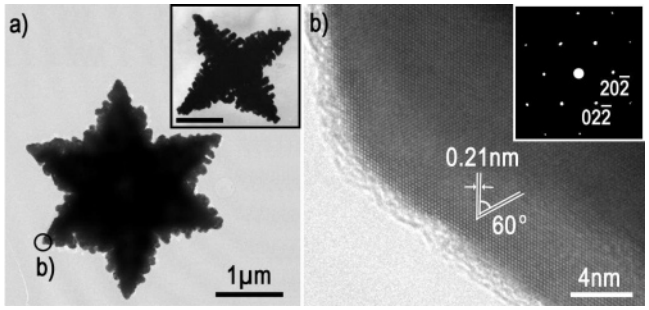

Figure 3. (a) Low-magnification TEM image of the architecture viewed from the tilted frontal perspective, showing that the architecture has 6-fold geometrical symmetry arms like a snowflake. Inset: TEM image of the architecture with 4-fold geometrical symmetry viewed from the diagonal perspective. Scale bar: 1 μm. (b) HRTEM image taken from the area labeled b in part a. Inset: the corresponding SAED pattern.

fraction (SAED). The TEM image of an individual architecture is shown in Figure 3a viewed from the tilted frontal perspective, from which one can clearly see that the architecture has six symmetric arms like a snowflake. The inset is the image viewed from the diagonal perspective, which shows the four symmetric arms. Figure 3b shows a HRTEM image taken from the labeled area in Figure 3a. The lattice spacing of 2.10 Å between each adjacent plane is in accordance with the spacing of the {100} crystal planes of cubic PbS. The sharp SAED spots (Figure 3b inset) reveal the single-crystallinity of the architecture. It is worth mentioning that the SAED patterns recorded along the same direction as the Figure 3b inset on different parts of the architecture, such as the trunk tips, the branch tips, and the central part, turn out to be the same, suggesting that the whole architecture is single-crystalline with the growth of the arms symmetrically along the six crystallographically equivalent directions [100]. The EDXA analysis also confirms that the product was pure PbS (Figure S1).

Although the exact mechanism for the L-cysteine-assisted formation of PbS nanocube-based pagoda-like hierarchical architectures is still under investigation, the interaction between Pb^{2+} and cysteine is undoubtedly significant. The function groups in the cysteine molecule such as $-NH_2$, $-COOH$, and $-SH$ have a strong tendency to interact with inorganic cations, which has been confirmed by Burford and co-workers on the basis of mass spectrometry. When mixing the L-cysteine and $Pb(Ac)_2$ solution, Pb^{2+} can interact with cysteine molecules to form precursor complexes. In the following process, the coordinate bond between L-cysteine and Pb^{2+} ruptures when the reaction temperature becomes higher (120 °C). The reactions taking place in the system can be described as follows:

$$Pb^{2+} + n\ \text{L-cysteine} \xrightarrow{\text{coordination}} [Pb(\text{L-cysteine})_n]^{2+}$$

$$[Pb(\text{L-cysteine})_n]^{2+} \xrightarrow{\text{Pb-S rupture}} PbS$$

To understand the growth mechanism of the pagoda-like structure, we've investigated the intermediate stages involved in the growth process by FESEM and FTIR, which are shown in Figures 4 and 5. When the $Pb(Ac)_2$ solution and L-cysteine solution are mixed for a period of time, a grayish-green suspension is obtained. The suspension has been confirmed by FTIR spectra (as shown in Figure 5a) to be the precursor formed by L-cysteine and $Pb(Ac)_2$. The peaks at 1555 and 1580 cm^{-1} are attributed to the characteristic peaks of the I and II bands for amino acids, from the diagnostic vibrations of acylamino ($-CO-NH_2-$) I and II bonding. The peaks around 3300 cm^{-1} are the characteristic peaks of the amido ($-NH_2$), while the

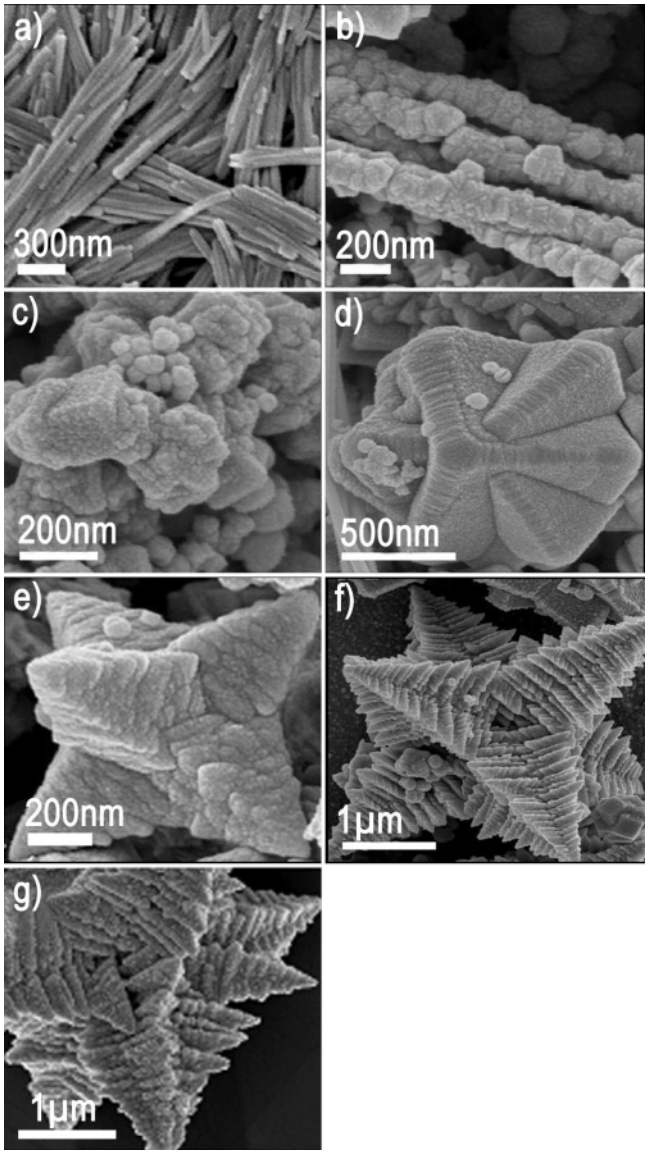

Figure 4. FESEM images showing the shape evolution of the intermediates: after hydrothermal treatment for (a) 0, (b) 1, (c) 1.5, (d) 2, (e) 2.5, (f) 3, and (g) 6 h.

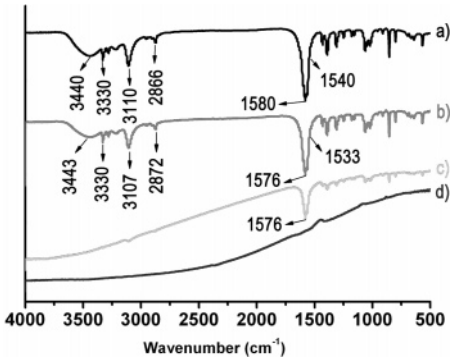

Figure 5. FTIR spectra of the intermediates collected after the reaction has proceeded for (a) 0, (b) 1, (c) 3, and (d) 6 h.

peaks at ca. 2800 cm^{-1} are believed to be the $-SH$ signal.[37] The corresponding XRD pattern also demonstrates that the precursor is composed of the complex of L-cysteine and $Pb(Ac)_2$ rather than PbS (Figure S2). The precursor turns out to have a bundle-like morphology (Figure 4a). Each of the bundles contains about 8−10 nanorods with a diameter of ca. 100 nm. Figure 4b shows the FESEM image of the intermediate

collected after reacting for 1 h. The bundles begin to disband, and the nanorods are released from the bundles. Meanwhile, the nanorods also show a tendency to decompose because their surfaces become coarse. When the reaction has proceeded for 1.5 h, a lot of nanoparticles accumulating and joining together grow out of the nanorods as shown in Figure 4c. As the reaction proceeds for 2 h, these particle-joint structures disappear and smooth large microcrystals form (Figure 4d). Such large microcrystals have six horns, which extend along the <100> directions (as shown in Figure 3b). When the reaction time is prolonged to 2.5 h, the intermediate becomes 4-fold symmetric star-shaped microcrystals (Figure 4e). When the reaction time reaches 3 h, hierarchical structures appear on the surface of the 4-fold star-shaped intermediate as presented in Figure 4f. After reacting for 6h, the microcrystals gradually evolve into nanocube-based pagoda-like hierarchical architectures, as shown in Figure 4g. The FTIR spectra (Figure 5) of the intermediates obtained at the time intervals of 0, 1, 3, and 6 h confirm that the precursor of the Pb^{2+} and L-cysteine complex shows a gradual decomposition exhausting as the reaction proceeds. Pure PbS can be obtained after hydrothermal treatment for 6 h.

Generally, the growth process of crystals includes two stages: an initial nucleating stage and a subsequent growth stage. The morphology and structure of the final product are determined by both the crystalline phase of the nuclei and the growth rate of the different crystal surface. It is well known that the surface energies of different crystallographic planes are usually different, and a general sequence is $\gamma\{111\} < \gamma\{100\} < \gamma\{110\}$.[38] But the intrinsic surface energy of cubic PbS {111} facets that contain Pb or S only is higher than its {100} facets, which contain mixed Pb/S.[39] The growth rates on different facets are dominated by the surface energy. As illustrated by Z. L. Wang, the shape of an fcc nanocrystal is determined mainly by the ratio (***R***) between the growth rates along the <100> and <111> directions,[38] for example, an octahedron bound by the most-stable {111} planes will form when $\boldsymbol{R} = 1.73$, and perfect cubes bound by the less-stable {100} planes will be produced if ***R*** is reduced to 0.58. The study on the intermediate clearly indicates that the biomolecule, L-cysteine, plays a crucial role: First, Pb^{2+} cations react with L-cysteine molecules to form complex bundles (Figure 4a). With increasing reaction time, the coordinate bonds between the hydrosulfide group and Pb^{2+} rupture because of the high reaction temperature and form the aggregated nanoparticles as observed in Figure 4b and c. Note that the IR peaks of −SH and the amino acid become weak, indicating that the ligands are gradually released and consumed in the reaction system (Figure 5b). Because the interaction between L-cysteine molecules and high-energy crystallography planes {110} is stronger than other low-energy planes of the nuclei, the <110> direction growth is thus prohibited. Meanwhile, L-cysteine molecules are preferentially absorbed on the {111} face because the surface energy of the {111} faces is higher than that of the {100} face, inducing a large ***R*** value, and resulting in the formation of the star-shaped microcrystal as shown in Figure 4d and e. The second nucleation can occur at the tips and edge area of the star-shaped microcrystal because of the higher energy of the tips, which has been reported by Kar and Huang, respectively.[3,23] In the FTIR spectra of the products after heating for 3 h, we found that signal of $-NH_2$ and −SH disappeared and the amino acid signal became very weak, which means that during the second nucleation stage the concentration of the L-cysteine and other ligands decreased drastically. Because the L-cysteine is always preferentially absorbed by the {111} faces and inhibits their growth, it is reasonable to deduce that the marked decrease of L-cysteine results in the inhibition on {111} faces. So the growth rate along [111] is thus favored and ***R*** is reduced to about 0.58, resulting in the formation of small nanocubes on the surface. On the basis of experimental results and discussion, a possible process for the formation of the PbS nanocube-based pagoda-like assemblies is proposed in Scheme 1.

SCHEME 1: Proposed Growth Process of PbS Nanocube-Based Pagoda-like Hierarchical Architectures

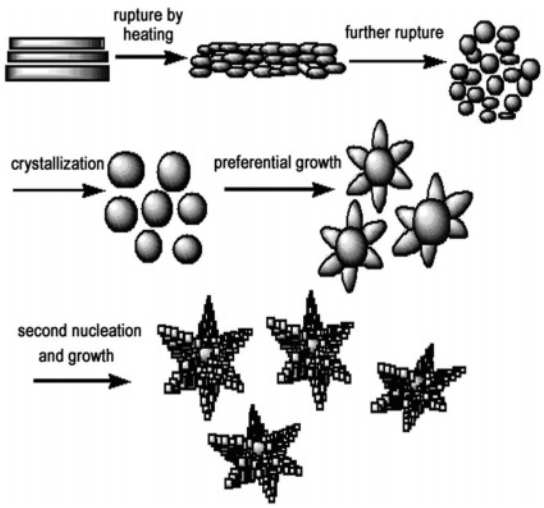

On the basis of the above systematic study and analysis of the mechanism for the formation of the pagoda-like architectures, the concentration of the reactants has a significant influence on the growth ratio ***R*** in the formation of PbS nuclei at an early stage. This result suggests that it is possible to control and tune the shape of PbS nanostructures by controlling the kinetic parameters of the reaction process. In order to provide more evidence supporting the above conclusion, we changed the concentration of the reactant and examined the morphology of the obtained products. When keeping other experimental parameters unchanged, but using only 0.031 g of $Pb(Ac)_2$ and 0.020 g of L-cysteine ($C_{cysteine} = 0.004$ M, molar ratio = 1:2), perfect nanocubes with an edge length of 100 nm are obtained in large scale as shown in Figure 6a and b. When the amounts

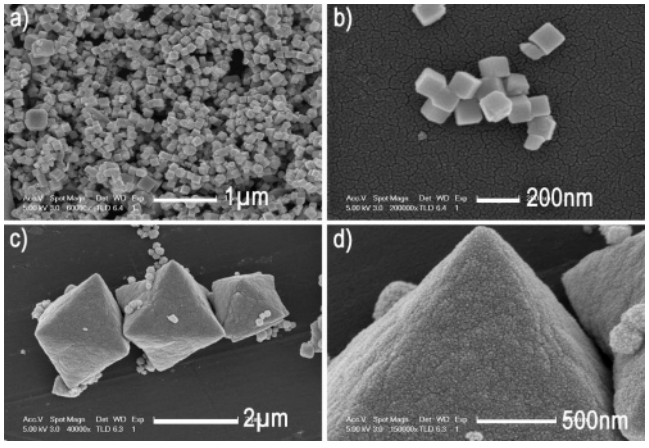

Figure 6. (a) Low- and (b) high-magnification FESEM images of the PbS nanocubes obtained with 0.031 g of $Pb(Ac)_2$ and 0.020 g of L-cysteine (with a 1:2 molar ratio) dissolved in 40 mL of deionized water maintaining at 120 °C for 6 h. (c) Low- and (d) high-magnification FESEM images of the PbS octahedrons obtained with 0.076 g of $Pb(Ac)_2$ and 0. 0.049 g of L-cysteine (with a 1:2 molar ratio) dissolved in 40 mL of deionized water maintaining at 120 °C for 6 h.

of $Pb(Ac)_2$ and cysteine are 0.076 and 0.049 g, respectively ($C_{cysteine}$ = 0.010 M, molar ratio = 1:2), PbS octahedrons (Figure 6c and d) can be readily achieved. The morphology evolution can be explained by the mechanism proposed above: as we reduce the amount of cysteine ($C_{cysteine}$ = 0.010 M), the prohibition on the {111} face is weakened, and the ***R*** value may be close to 1.73, octahedrons are thus obtained. Alternatively, if the amount of the cysteine is further reduced ($C_{cysteine}$ = 0.004 M), then the growth rate on the {111} face is favored and the ***R*** value may be reduced to 0.58 and nanocubes are synthesized.

4. Conclusions

In summary, PbS pagoda-like hierarchical architectures have been prepared by using a simple L-cysteine-assisted technique. The process for the formation of the PbS pagoda-like architectures is carefully studied and discussed. A novel second nucleation phenomenon has been observed, which is responsible for the formation of such hierarchical structures. It is suggested that a mimetic biomineralization process occurs during the formation of as-prepared hierarchical architectures because the biomolecule L-cysteine exerts coordination, oriented nucleation of crystals, and the morphology modulating effect. The growth ratio ***R*** has a great influence on the morphology of the PbS products. By adjusting the concentration of the reagents, the ***R*** value can be tuned and various shapes of the PbS (nanocubes and octahedron microcystal) can thus be prepared. On the basis of the studies on shape evolution, this approach is expected to be employed for shape-controlled synthesis of other functional materials.

Acknowledgment. This work was financially supported by the National Natural Science Foundation of China (no. 20621061) and the state key project of fundamental research for nanomaterials and nanostructures (2005CB623601).

Supporting Information Available: EDAX analysis of the PbS pagoda-like hierarchical architectures and XRD pattern of the precursor collected from the mixed L-cysteine and $Pb(Ac)_2$ suspension. This material is available free of charge via the Internet at http://pubs.acs.org.

References and Notes

(1) Xia, Y. N.; Yang, P. D.; Sun, Y. G.; Wu, Y. Y.; Mayers, B.; Gates, B.; Yin, Y. D.; Kim, F.; Yan, H. Q. *Adv. Mater.* **2003**, *15*, 353.

(2) Xiao, Z. L.; Han, C. Y.; Kwok, W. K.; Wang, H. H.; Welp, U.; Wang, J.; Crabtree, G. W. *J. Am. Chem. Soc.* **2004**, *126*, 2316.

(3) Zhao, P. T.; Wang, J. M.; Cheng, G. E.; Huang, K. X. *J. Phys. Chem. B* **2006**, *110*, 22400.

(4) (a) Hayat, M. A. *Colloidal Gold: Principles, Methods, and Applications*; Academic Press: San Diego, CA, 1991. (b) Creighton, J. A.; Blatchford, C. G.; Albrecht, M. G. *J. Chem. Soc., Faraday Trans. 2* **1979**, *75*, 790. (c) Henglein, A.; Ershov, B. G.; Malow, M. *J. Phys. Chem.* **1995**, *99*, 14129. (d) Curtis, A. C.; Duff, D. G.; Edwards, P. P.; Jefferson, D. A.; Johnson, B. F. G.; Kirkland, A. I.; Wallace, A. S. A*ngew. Chem., Int. Ed. Engl.* **1988**, *27*, 1530.

(5) Murray, C. B.; Norris, D. J.; Bawendi, M. G. *J. Am. Chem. Soc.* **1993**, *115*, 8706. (b) Chestoy, N.; Hull, R.; Brus, L. E. *J. Chem. Phys.* **1986**, *85*, 2237. (c) Wang, Y.; Herron, N. *J. Phys. Chem.* **1991**, *95*, 525. (d) Kavan, L.; Gratzel, M.; Rathousky, J.; Zukal, A. *J. Electrochem. Soc.* **1996**, *143*, 394. (e) Spanhel, L.; Anderson, M. A. *J. Am. Chem. Soc.* **1991**, *113*, 2826. (f) Heath, J. R.; Williams, R. S.; Shiang, J. J.; Wind, S. J.; Chu, J.; D' Emic, C.; Chen, W.; Stanis, C. L.; Bucchignano, J. J. *J. Phys. Chem.* **1996**, *100*, 3144.

(6) Feltin, N.; Pileni, M. P. *Langmuir* **1997**, *13*, 3927.

(7) Mirkin, C. A. *Inorg. Chem.* **2000**, *39*, 2258.

(8) Hu, J.; Odom, T. W.; Lieber, C. M. *Acc. Chem. Res.* **1999**, *32*, 435.

(9) Dekker, C. *Phys. Today* **1999**, *52*, 22.

(10) Heath, J. R.; Kuekes, P. J.; Snider, G. S.; Williams, R. S. *Science* **1998**, *280*, 1716.

(11) Tahir, M. N.; Zink, N.; Eberhardt, M.; Therese, H. A.; Faiss, S.; Janshoff, A.; Kolb, U.; Theato, P.; Tremel, W. *Small* **2007**, *3*, 829.

(12) Lowenstam, H. A.; Weiner, S. *On Biomineralisation*; Oxford Univ. Press: New York, 1989.

(13) Sundar, V. C.; Yablon, A. D.; Grazul, J. L.; Ilan, M.; Aizenberg, J. *Nature* **2003**, *424*, 899.

(14) Politi, Y.; Arad, T.; Klein, E.; Weiner, S.; Addadi, L. *Science* **2004**, *306*, 1161.

(15) Aizenberg, J.; Hendlen, G. J. *J. Mater. Chem.* **2004**, *14*, 2066.

(16) Aizenberg, J.; Weaver, J. C.; Thanawala, M. S.; Sundar, V. C.; Morse, D. E.; Fratzl, P. *Science* **2005**, *309*, 275.

(17) Aizenberg, J.; Sundar, V. C.; Yablon, A. D.; Weaver, J. C.; Chen, G. *Proc. Natl. Acad. Sci. U.S.A.* **2004**, *101*, 3358.

(18) Pouget, E.; Dujardin, E.; Cavalier, A.; Moreac, A.; Valery, C.; Marchi-Artzner, V.; Weiss, T.; Renault, A.; Paternostre, M.; Artzner, F. *Nat. Mater.* **2007**, *6*, 434.

(19) Woesz, A.; Weaver, J. C.; Kazanci, M.; Dauphin, Y.; Aizenberg, J.; Morse, D.; Fratzl, P. *J. Mater. Res.* **2006**, *21*, 2068.

(20) Mann, S. *Nature* **1988**, *332*, 119.

(21) Cavalli. S.; Popescu, D. C.; Tellers, E. E.; Vos, M. R. J.; Pichon, B. P.; Overhand, M.; Rapaport, H.; Sommerdijk, N. A. J. M.; Kros, A. *Angew. Chem., Int. Ed.* **2006**, *45*, 739.

(22) Ni, X. M.; Zhao, Q. B.; Zhang, D. E.; Zhang, X. J.; Zheng, H. G. *J. Phys. Chem. C* **2007**, *111*, 601.

(23) Kar, S.; Chaudhuri, S. *J. Phys. Chem. B* **2006**, *110*, 4542.

(24) Zhang, Z. H.; Lee, S. H.; Vittal, J. J.; Chin, W. S. *J. Phys. Chem. B* **2006**, *110*, 6649.

(25) Zhang, H.; Zuo, M.; Tan, S.; Li, G. P.; Zhang, S. Y. *Nanotechnology* **2006**, *17*, 2931.

(26) Zhao, N. N.; Qi, L. M. *Adv. Mater.* **2006**, *18*, 359.

(27) Zhou, G. J.; Lu, M. K.; Xiu, Z. L.; Wang, S. F.; Zhang, H. P.; Zhou, Y. Y.; Wang, S. M. *Phys. Chem. B* **2006**, *110*, 6543.

(28) Cao, H. Q.; Wang, G. Z.; Zhang, S. C.; Zhang, X. R. *Nanotechnology* **2006**, *17*, 3280.

(29) Lu, Q. Y.; Gao, F.; Komarneni, S. *Nanotechnology* **2006**, *17*, 2574.

(30) Zhang, C.; Kang, Z. H.; Shen, E. H.; Wang, E. B.; Gao, L.; Luo, F.; Tian, C. G.; Wang, C. L.; Lan, Y. *J. Phys. Chem. B* **2006**, *110*, 184.

(31) Cornacchio, A. L. P.; Jones, N. D. *J. Mater. Chem.* **2006**, *16*, 1171.

(32) Zhang, L.; Gaponik, N.; Muller, J.; Plate, U.; Weller, H.; Erker, G.; Fuchs, H.; Rogach, A. L.; Chi, L. F. *Small* **2005**, *1*, 524.

(33) Lu, Q. Y.; Gao, F.; Komarneni, S. *J. Am. Chem. Soc.* **2004**, *126*, 54.

(34) Lu, Q. Y.; Gao, F.; Komarneni, S. *Langmuir* **2005**, *21*, 6002.

(35) Zhang, B.; Ye, X. C.; Dai, W.; Hou, W. Y.; Xie, Y. *Chem.—Eur. J.* **2006**, *12*, 2337.

(36) Zuo, F.; Zhang, B.; Tang, X. Z.; Xie, Y. *Nanotechnology*, **2007**, *18*, 215608.

(37) Zhang B.; Ye X. C.; Hou W. Y.; Zhao Y.; Xie Y. *J. Phys. Chem. B* **2006**, *110*, 8978.

(38) Wang, Z. L. *J. Phys. Chem. B* **2000**, *104*, 1153.

(39) Jun, Y. W.; Lee, J. H.; Choi, J. S.; Cheon, J. *J. Phys. Chem. B* **2005**, *109*, 14795.